ACS OMEGA

http://pubs.acs.org/journal/acsodf

Article

Prediction Model of Dry Fertilizer Crushing Force Based on P-DE-SVM

Hongjian Zhang, Xuemei Liu, Shuangxi Liu, Hao Jiang, Chunbao Xu, and Jinxing Wang*

Cite This: *ACS Omega* 2021, 6, 3612−3624

Read Online

ACCESS | Metrics & More | Article Recommendations

ABSTRACT: The accurate prediction of fertilizer crushing force could reduce the crushing rate in the process of transportation and utilization and ensure the efficient utilization of the fertilizer so as to realize the sustainable and clean production of crops. To achieve this goal, a fertilizer crushing force prediction model based on the shape characteristics was proposed in this paper using the Pearson correlation coefficient, differential evolution algorithm, and the support vector machine (P-DE-SVM). First, the shape characteristics and crushing force of fertilizers were measured by an independently developed agricultural material shape analyzer and digital pressure gauge, and the shape characteristics related to the fertilizer crushing force were proposed based on the Pearson correlation coefficient. Second, a fertilizer crushing force prediction model based on a support vector machine was constructed, in which the optimal kernel function was the radial basis function. Finally, a differential evolution algorithm was proposed to optimize the internal parameters of the fertilizer-crushing force prediction model, and at the same time, a fertilizer granularity inspection range was calculated. The experimental results showed that the maximum error rate of the fertilizer crushing force prediction model was between −10.4 and 10.9%, and the fertilizer granularity inspection range was reasonable. The proposed prediction model in this paper could lay a solid foundation for fertilizer production and quality inspection, which would help reduce fertilizer crushing and improve fertilizer utilization to realize the sustainable and clean production of crops.

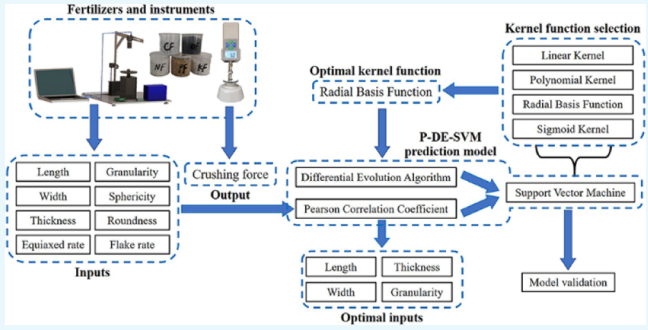

1. INTRODUCTION

As one of the most important basic substances in agricultural production, fertilizers play an important role in ensuring the safety of food production and the high yield of agriculture.[1] China is the world's major fertilizer production and application country. In 2018, the total output of agricultural fertilizers reached 54.18 million tons, and the application amount of agricultural fertilizers reached 56.534 million tons, accounting for around 1/3 of the world's total.[2] Fertilizers are easily broken during transportation and utilization, causing fertilizer to cake, affecting the diffusion of fertilizer nutrients, and resulting in low fertilizer utilization.[3,4] Therefore, accurate prediction of fertilizer crushing force is of great significance for reducing fertilizer waste and improving fertilizer utilization.

The particle shape affects the mechanical and flow behavior of the granular material.[5,6] For example, corner sand tends to have high shear strength, stress concentration at the contact, resistance to flow, and liquefaction.[7] Besides, particle morphology also affects the interaction of particles with fluid and air, such as drag coefficient and mineral floatability.[8] Therefore, shape characteristic is an important parameter for predicting and controlling the properties of granular materials. Fertilizer is an important kind of agricultural granule. Its shape characteristics affect the appearance quality, strength, fluidity, and the effect of machine-seeded fertilizer and have important significance for the design and research of agricultural machinery.[9,10]

Kan et al.[11] found that the higher the sphericity of the fertilizer, the denser the fertilizers, the higher the strength of the fertilizer; the higher the roundness of the fertilizer, the smoother and more uniform the fertilizer, the greater the porosity of the fertilizer, and the faster the heat dissipation, the better the fluidity. Research by Hofstee and Huisman[12] found that the five physical properties that affect fertilizer movement are fertilizer granularity, strength, friction coefficient, recovery coefficient, and aerodynamic resistance. Among them, the strength of the fertilizer indirectly affects its movement, and fertilizers with low strength will rupture during movement, resulting in changes in the size of

Received: October 20, 2020
Accepted: January 18, 2021
Published: January 29, 2021

fertilizers, affecting the distribution of particle nutrients. Cao et al.[13] found through research that the shape of the fertilizer and the pore structure formed by fertilizer accumulation affect the diffusion of fertilizer salt ions, which in turn affects fertilizer performance. Basu and Kumar[14] and Terry[15] found through research that the granularity of fertilizer affects the separation and release time of fertilizer nutrients. Through model tests, Hoffmeister, Watkins, and Silverberg[16] found that the difference in fertilizer granularity, shape, and density affects the changing trend of nutrient separation during the transportation and spread of blended fertilizers.

Fertilizers are irregularly shaped particles, and it is difficult to accurately measure their shape characteristics manually. With the rapid development of computer and software technology, it is possible to measure particle shape with the help of computer technology. Fernlund[17] measured the axial length of the long axis, the middle axis, and the short axis of the coarse aggregate through the 3D image analysis method, and the result showed that the measurement result of this method has a good correlation with the measurement result of the Danish box. Zhang, Ye, Chen, and Li[18] used digital image technology to measure and evaluate the shape of gravel particles.

In recent years, artificial intelligence and machine learning theories have been widely studied and applied. Machine learning methods based on statistical theory, such as neural networks, decision trees, and support vector machines, show excellent performance when dealing with classification and prediction problems.[19] Compared with the neural network, the support vector machine is constructed according to the structural risk minimization criterion, which can reduce the probability of model overfitting and make up for the shortcomings of the neural network. The insensitive area in the structure can absorb the small-scale random fluctuations that appear in the random response, so it still has a good predictive ability in the case of a small amount of data.[20] Support vectors have developed rapidly in various fields, such as small samples, nonlinearity, and pattern recognition, and can be extended to other practical problems such as function fitting.[21]

Stevens, Nocita, Tóth, Montanarella, and van Wesemael[22] used support vector machines and Cubist to predict organic carbon. Lu, Zhang, Wu, Ma, Liao, and Hu[23] built a prediction model for the cutting speed, feed rate, depth of cut, and surface roughness in the milling of vermicular graphite cast iron based on support vector machines and verified the validity of the prediction model. Li, Gui, and Zhu[24] used convolutional neural networks to extract the features of foam images and built a fault diagnosis model in the flotation process based on support vector machines.

Based on the above research studies, it is found that the shape characteristics affect fertilizer crushing force. Fertilizers with low crushing force are more likely to be crushed during transportation and utilization. Crushed fertilizers affect nutrient diffusion, reduce fertilizer utilization, and pollute the environment, which is not conducive to the sustainable production of crops. So far, there are few studies on support vector machines in fertilizer crushing force prediction models. To predict the fertilizer crushing force and reduce the fertilizer crushing rate, the triaxial characteristics, roundness, sphericity, granularity, and crushing force of the fertilizer were measured by an agricultural material shape analyzer and digital pressure gauge. Based on the Pearson correlation coefficient, the support vector machine, and the improved differential evolution algorithm (P-DE-SVM), a fertilizer crushing force prediction model was constructed, and the fertilizer granularity inspection range was calculated.

2. MATERIALS AND METHODS

2.1. Description Method of Fertilizer Shape Characteristics. *2.1.1. Triaxial Characteristics.* The macroscopic outline of particles is usually represented by three mutually perpendicular axes, namely, the long axis, the middle axis, and the short axis, which are equivalent to the dimensions of the length, width, and thickness of the particle. In a natural and stable state, the length of the particles refers to the largest dimension in the plane projection graph, the width refers to the linear dimension perpendicular to the length direction, and the thickness refers to the linear dimension perpendicular to the length and width directions. The relationship between the three axes of particles can be expressed by the equiaxed rate and flake rate[25]

$$k = b/a \tag{1}$$

$$\lambda = c/b \tag{2}$$

where k is the particle equiaxed rate, λ is the particle flake rate, a is the particle length, b is the particle width, and c is the particle thickness.

2.1.2. Roundness. The roundness (σ) reflects the sharpness of the edges and corners of the particles. The particle roundness is defined as[26]

$$\sigma = 4\pi A/L^2 \tag{3}$$

where L is the particle projection contour circumference, and A is the particle projection area.

2.1.3. Sphericity. Sphericity (φ) reflects how close the particle is to the sphere. The particle sphericity is defined as[27]

$$\varphi = \sqrt[3]{v/v_s} \tag{4}$$

According to the definition of the particle sphericity, if the particle is equated as an ellipsoid, the equivalent volume v of the particle is[28]

$$v = (\pi/6)abc \tag{5}$$

Substituting formula 4 can obtain the calculation formula of particle sphericity

$$\varphi = \sqrt[3]{v/v_s} = \sqrt[3]{(\pi/6)abc/(\pi/6)a^3} = \sqrt[3]{bc/a^2} \tag{6}$$

where v is the equivalent volume, and v_s is the volume of the smallest sphere circumscribed by the particle (a sphere whose diameter is length a).

2.1.4. Granularity. Granularity (d) is used to indicate the size of the particles, which can be expressed as the single size of a single particle or the average granularity of a group of particles. The granularity d of a single spheroid is[29]

$$d = \sqrt[3]{6v/\pi} = \sqrt[3]{abc} \tag{7}$$

where d is the granularity.

2.2. Measurement Method of Fertilizer Shape Characteristics. *2.2.1. Measurement of Fertilizer Shape Characteristics.* We use the agricultural material shape analyzer independently developed to obtain the fertilizer shape parameters. The structure of the machine is shown in

https://dx.doi.org/10.1021/acsomega.0c05120
ACS Omega 2021, 6, 3612−3624

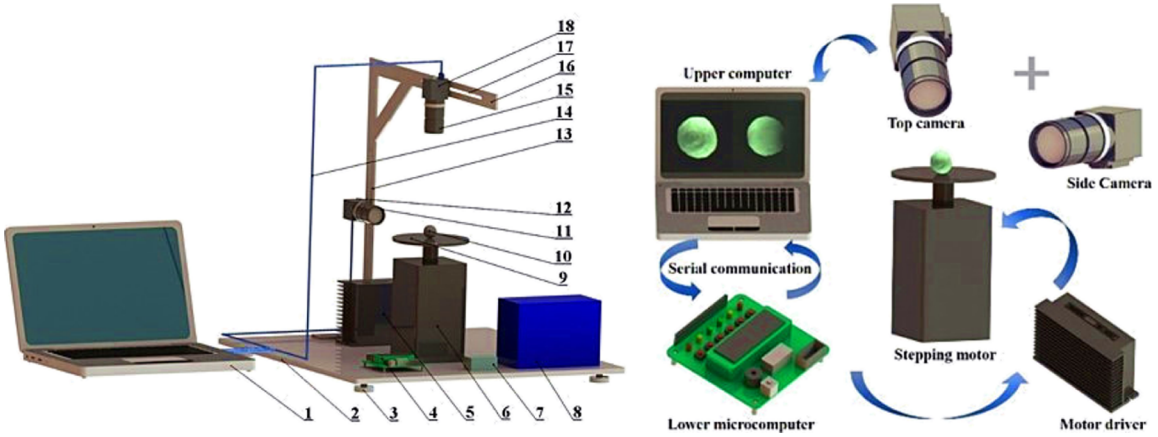

Figure 1. Three-dimensional structure of the machine and fertilizer collection process. 1. Upper computer 2. Base 3. Adjusting foot 4. Lower microcomputer 5. Driver 6. Stepper motor 7. Power conversion module 8. Power supply 9. Objective stage 10. Fertilizer to be tested 11. Side lens 12. Side camera 13. Side notch 14. Data transmission line 15. Top lens 16. Camera adjustment frame 17. Top notch 18. Top camera.

Figure 1. It is mainly composed of the base, the objective stage, the stepping motor, the top camera, the top lens, the side camera, the side lens, the power supply, the upper computer, and the lower microcomputer. Among them, the stepping motor is an 86BYG250H two-phase motor produced by Pfide Electric Co., Ltd., with a step angle of 1.8°. The top camera and the side camera are both FL-U3-13S2C-CS industrial cameras produced by Point Grey, and the resolution is 1328 × 1048. The top lens and the side lens are both FL-CC3516-2M fixed-focus lenses produced by Pentax, with a focal length of 35 mm.

The agricultural material shape analyzer uses intermittent static collection mode to automatically collect the top and side images of a single fertilizer. The objective stage is engraved with a cross calibration, and the fertilizer to be tested is first placed at the center of cross calibration. The objective stage is connected to the stepping motor through a half-circle key, and the lower microcomputer controls the rotation of the stepping motor to drive the stage to achieve the rotation of the fertilizer to be tested. The stepping motor stops after the set angle is rotated, the lower microcomputer sends a rotation completion command to the upper computer through the serial port, and the upper computer controls the top and side cameras to collect the top and side images of the fertilizer to be tested. After the acquisition is completed, the upper computer sends an image acquisition completion command to the lower microcomputer through the serial port, and the lower microcomputer controls the stepping motor to rotate again. We repeat this process until the top and side images of the target number are obtained. The collection process is shown in Figure 1.

To establish the relationship between the actual size of the fertilizer and the pixels, the image information of the calibration target (10 mm × 10 mm black square) is collected, and the grayscale and binarization process is performed. The process is shown in Figure 2. In the threshold image, the target area is black and the threshold value is 0. The threshold image is traversed by pointer scanning, and the number of rows of all pixels that meet the defined threshold is counted N_0 = 550. According to formula 8, the actual length represented by a single pixel (L_0) is 0.018 mm. After the length calibration and the images of the single fertilizer are all collected, the upper computer analyzes the top and side images to obtain the basic parameters of the

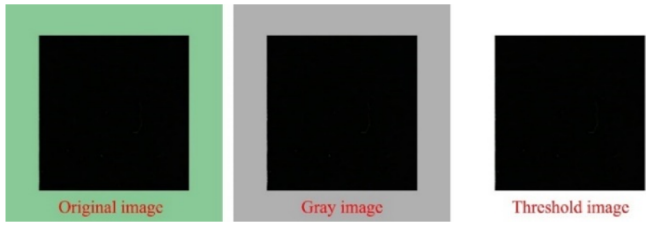

Figure 2. Length calibration. Note: *a*, *b*, and *c* refer to the length, width, and thickness of fertilizers, respectively.

fertilizer, as shown in Figure 3. The specific process is as follows:

(1) The top and side images are grayscale and Gamma-corrected, and the edge detection is performed on the top and side grayscale images of the fertilizer using the Canny operator to obtain the top and side contour images of the fertilizer.

(2) In the top contour image of the fertilizer, the parameters such as the perimeter L, area A, and the minimum circumscribed rectangle of the top contour of the fertilizer are obtained. Because the length of the minimum circumscribed rectangle of the fertilizer contour represents the maximum size of the particle in the top view projection, the width of the minimum circumscribed rectangle represents the minimum size of the fertilizer in the top-view projection. Therefore, the length and width of the minimum circumscribed rectangle are, respectively, equivalent to the length a and width b of the fertilizers, and then, the fertilizer equiaxed ratio k and roundness σ are calculated according to eqs 1 and 3

(3) In each side image of the fertilizer, the minimum circumscribed rectangle parameters of the side contour are obtained. The width of the minimum circumscribed rectangle represents the straight-line size of the fertilizer perpendicular to the length and width direction. To reduce the error, the average value of the minimum circumscribed rectangle width of all side contours is equivalent to the particle thickness c, and then, the fertilizer flake rate λ, sphericity φ, and granularity d are calculated according to formulas 2, 6, and 7

https://dx.doi.org/10.1021/acsomega.0c05120
ACS Omega 2021, 6, 3612−3624

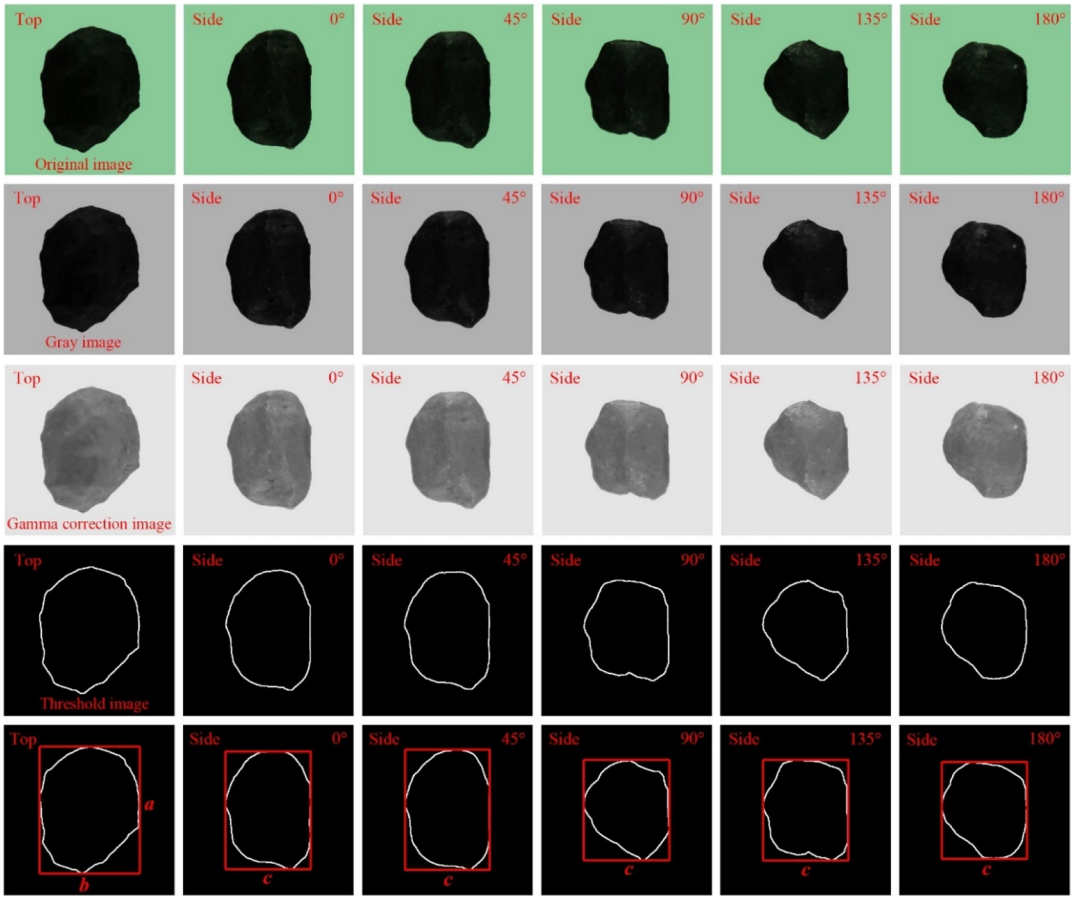

Figure 3. Extraction process of particle shape parameters.

$$L_0 = 10/N_0 \quad (8)$$

where L_0 is the actual length value represented by a single pixel, and N_0 is the number of rows of all pixels that meet the defined threshold.

2.2.2. Measurement of Fertilizer Crushing Force. The crushing force of the fertilizer is obtained by the SGW-J digital pressure gauge produced by Shanghai Siwei Instrument Manufacturing Co., Ltd. The structure of the machine is shown in Figure 4. It is mainly composed of the digital operation interface, the objective stage, the pressure head, the hand wheel, the column, the adapter plate, and the base. Among them, the force sensitivity is 0.1 N, the relative velocity of the pressure head is about 0.25 mm/s, and the diameter of the objective stage is 17.5 mm.

Figure 4. Structure of the digital pressure gauge. 1. Digital operation interface 2. Pressure head 3. Objective stage 4. Hand wheel 5. Adapter plate 6. Column 7. Base.

First, the fertilizer was randomly placed on the objective stage, and the peak value measurement mode was selected. Second, the hand wheel was turned to move the objective stage upward slowly, and the fertilizer touched the pressure head. At this time, the digital display interface showed the pressure is 0 N. Third, the hand wheel was continued to be turned, the fertilizer was pressed by the pressure head, and the digital display interface showed the pressure value increase process in real time. Finally, the hand wheel was continued to be turned until the fertilizer was completely crushed, the pressure was no longer increased, and the digital display interface showed the maximum pressure value in the whole process.

2.3. Construction of the Crushing Force Prediction Model. This paper uses an agricultural material shape analyzer and a digital pressure gauge to measure the shape characteristics and crushing force of different fertilizers. The prediction model of the fertilizer crushing force (P-DE-SVM) is constructed through a support vector machine combined with the Pearson correlation coefficient and the differential evolution algorithm. The model of the overall process is shown in Figure 5.

3. RESULTS AND DISCUSSION

3.1. Data Acquisition and Preprocessing. According to the different nutrients in fertilizers, fertilizers can be divided into NF (N fertilizer), PF (P fertilizer), KF (K

https://dx.doi.org/10.1021/acsomega.0c05120
ACS Omega 2021, 6, 3612−3624

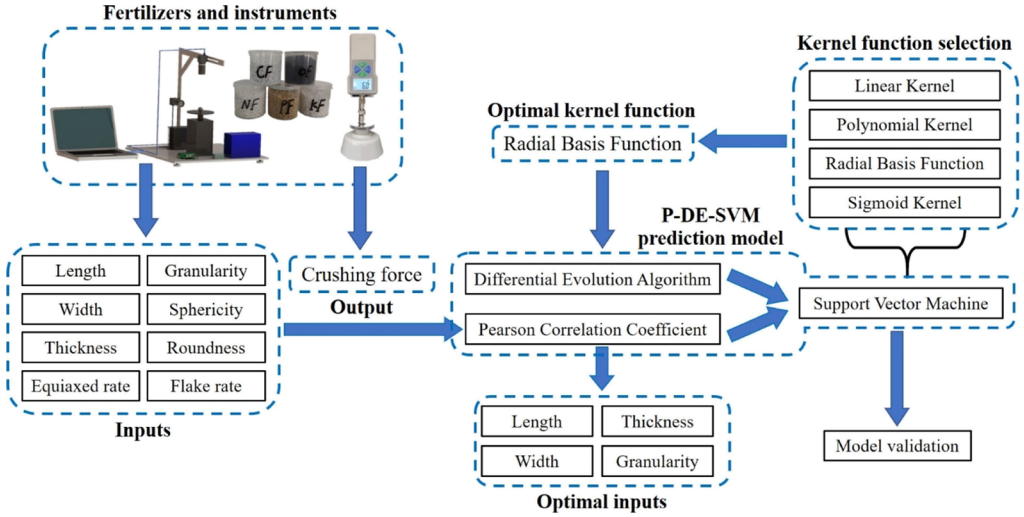

Figure 5. Construction process of the prediction model.

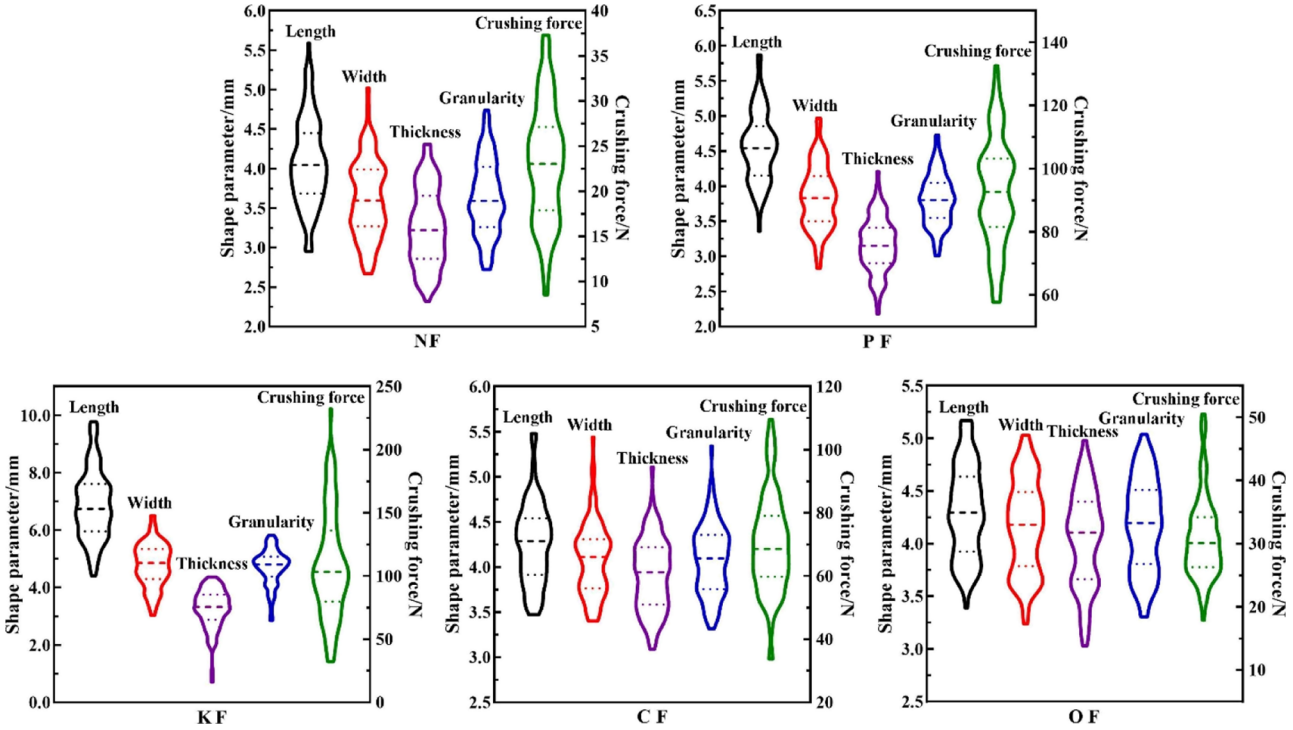

Figure 6. Shape characteristics and crushing force distribution of different fertilizers.

fertilizer), CF (compound fertilizer), and OF (organic fertilizer).[30] Among the NF produced by Sinofert Holding Limited, PF produced by Yuntianhua Group Co., Ltd., KF produced by Luxi Chemical Group Co., Ltd., CF produced by Stanley Agricultural Group Co., Ltd., and OF produced by Xinyangfeng Agricultural Technology Co., Ltd., 100 particles of each fertilizer were collected by random sampling from the same production batch, and a total of 500 particles were used as test samples. In the experiment, taking this sample as the research object, the shape parameters and crushing force were immediately measured by the agricultural material shape analyzer and digital pressure gauge. At the same time, other fertilizers in the same batch were dried to measure the density and moisture content. Among the same kind of fertilizers, the moisture, density, and other physical parameters were the same, except for the shape characteristics.

The densities of NF, PF, KF, CF, and OF were 1268, 1283, 1279, 1300, and 1155 kg/m^3, respectively. The moisture contents were 2.32, 2.19, 2.25, 1.14, and 5.25%, respectively. The distribution of length, width, thickness, granularity, and crushing force is shown in Figure 6. To verify the accuracy of the measurement, the statistical calculations were first performed on the test data, and the maximum, minimum, average, range, and standard deviation of each parameter of the fertilizer to be tested were obtained. The results are shown in Table 1. Among them, the average and standard deviation are

https://dx.doi.org/10.1021/acsomega.0c05120
ACS Omega 2021, 6, 3612−3624

Table 1. Different Fertilizer Parameters

	item	length a/mm	width b/mm	thickness c/mm	granularity d/mm	equiaxed rate k	flake rate λ	roundness σ	sphericity φ	crushing force s/N
NF	maximum	5.590	5.020	4.310	4.740	0.985	0.988	0.984	0.984	37.300
	minimum	2.950	2.670	2.320	2.723	0.615	0.683	0.681	0.670	8.500
	average	4.081	3.615	3.255	3.630	0.889	0.901	0.893	0.892	23.078
	range	2.640	2.350	1.990	2.017	0.370	0.304	0.303	0.315	28.800
	standard deviation	0.550	0.493	0.487	0.471	0.068	0.063	0.052	0.054	6.476
PF	maximum	5.870	4.970	4.210	4.730	0.972	0.972	0.955	0.955	132.650
	minimum	3.360	2.830	2.180	3.009	0.665	0.587	0.716	0.715	57.700
	average	4.565	3.842	3.167	3.807	0.844	0.830	0.839	0.837	92.599
	range	2.510	2.140	2.030	1.721	0.307	0.385	0.239	0.240	74.950
	standard deviation	0.493	0.445	0.386	0.358	0.072	0.098	0.053	0.054	16.883
KF	maximum	9.780	6.500	4.370	5.828	0.992	0.994	0.918	0.920	232.450
	minimum	4.410	3.040	1.250	3.031	0.442	0.303	0.430	0.431	32.350
	average	6.879	4.784	3.279	4.721	0.709	0.696	0.704	0.697	108.549
	range	5.370	3.460	3.120	2.796	0.550	0.691	0.488	0.489	200.100
	standard deviation	1.190	0.742	0.641	0.580	0.130	0.148	0.091	0.092	41.938
CF	maximum	5.480	5.440	5.110	5.341	0.998	0.998	0.997	0.997	109.550
	minimum	3.470	3.400	3.090	3.316	0.770	0.785	0.804	0.804	33.750
	average	4.263	4.091	3.914	4.085	0.961	0.957	0.960	0.960	70.166
	range	2.010	2.040	2.020	2.025	0.228	0.212	0.194	0.193	75.800
	standard deviation	0.442	0.396	0.397	0.386	0.043	0.040	0.037	0.037	15.182
OF	maximum	7.250	5.810	4.450	2.670	0.992	0.996	0.978	0.978	50.500
	minimum	3.440	3.020	2.580	0.320	0.590	0.863	0.676	0.660	17.900
	average	5.142	4.208	3.478	1.007	0.828	0.970	0.830	0.826	30.931
	range	3.810	2.790	1.870	2.350	0.402	0.133	0.302	0.318	32.600
	standard deviation	0.779	0.531	0.419	0.478	0.103	0.027	0.070	0.073	6.413

Table 2. Results of the Grubbs Test

index		length a	width b	thickness c	circumference L	area A	crushing force s
T_{Max}	NF	2.745	2.853	2.167	2.622	2.256	2.358
	PF	2.646	2.535	2.705	3.012	2.891	2.580
	KF	2.437	2.350	3.167	2.234	2.287	2.912
	CF	2.751	3.003	3.010	2.479	2.658	3.205
	OF	2.113	2.128	2.255	2.473	2.183	1.994

$$\overline{x} = \frac{\sum_{i=1}^{n} x_i}{n} \tag{9}$$

$$S = \sqrt{\frac{\sum_{i=1}^{n} (x_i - \overline{x})^2}{n-1}} \tag{10}$$

where x_i is the sample value, n is the total number of samples, $\overline{x}$ is the sample average, and S is the sample standard deviation.

It can be seen from Figure 6 and Table 1 that the distribution of length, width, thickness, granularity, and crushing force of NF, PF, CF, and OF is close to the bell-shaped distribution with the middle thickness and narrow sides; the granularity distribution is 2.723−4.740, 3.009−4.730, 3.316−5.341, and 3.306−5.040 mm, the crushing force is between 8.500 and 37.300 N, 57.700 and 132.650 N, 33.750 and 109.550 N, 17.900 and 50.500 N; and the distribution of length, width, granularity, and crushing force of KF is close to the middle thickness and narrow bell-shaped distribution on both sides. Its granularity distribution is between 3.031 and 5.828 mm, and the crushing force distribution is between 32.350 and 232.450 N.

To eliminate the abnormal data caused by negligent error, this study uses the Grubbs test method to test the discrete value of the directly measured raw data. First, the test data are sorted from small to large to obtain the average value and standard deviation of the data. Second, the statistic T_i is calculated according to formula 11, and the maximum value T_{Max} is obtained, and the results are shown in Table 2. Finally, the statistic T_{Max} is compared with the critical value $T_{\alpha,n}$ in the Grubbs test table (α is the significance level, and n is the sample size). If $T_{Max} \geq T_{\alpha,n}$, it means that x_i is a discrete value and must be discarded; otherwise, it should be retained.

$$T_i = \frac{\overline{x} - x_i}{S} (i = 1, 2, 3, \ldots, 100) \tag{11}$$

where T_i is the statistic value.

We query the Grubbs test value table, take $\alpha = 0.05$, $n = 100$, and $T_{0.05,100} = 3.207$, and compare the maximum value T_{Max} under each factor in Table 2 with $T_{0.05,100}$. We find that

https://dx.doi.org/10.1021/acsomega.0c05120
ACS Omega 2021, 6, 3612−3624

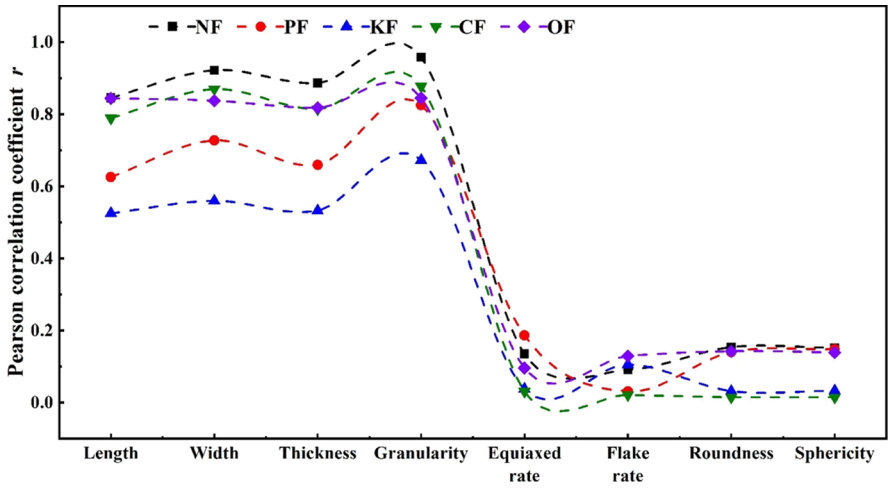

Figure 7. Correlation between shape characteristics and crushing force.

the data in each group are all less than $T_{0.05,100}$, so the original data in the group has no discrete value, which proves that the data is valid and accurate.

3.2. Pearson Correlation Coefficient. The Pearson correlation coefficient is a statistical method that accurately measures the closeness of the relationship between two variables.[31,32] It can reflect the strength of the linear correlation between the two variables. For variables $M = [m_1, m_2, ..., m_n]^T$ and $N = [n_1, n_2, ..., n_n]^T$, the calculation formula of the Pearson correlation coefficient is:

$$r = \frac{\sum_{i=1}^{n}(m_i - \overline{m})(n_i - \overline{n})}{\sqrt{\sum_{i=1}^{n}(m_i - \overline{m})^2 (n_i - \overline{n})^2}} \tag{12}$$

In formula 12, m_i and n_i are variable values and $\overline{m}$ and $\overline{n}$ are average values.

The value range of the correlation coefficient r is $-1 \le r \le 1$. The closer $|r|$ is to 1, the higher the correlation between m and n. If $r = -1$, it means that there is a completely negative linear correlation between m and n; if $r = 1$, it means that there is a completely positive linear correlation between m and n; if $r = 0$, it means that there is no linear correlation between m and n. In general, when $|r| \ge 0.8$, it can be regarded as high correlation; when $0.5 \le |r| < 0.8$, it can be regarded as moderate correlation; when $0.3 \le |r| < 0.5$, it can be regarded as low correlation; when $|r| < 0.3$, it indicates that the linear correlation between the two variables is extremely weak and can be regarded as a nonlinear correlation.

To accurately measure the correlation between fertilizer shape characteristics and crushing force, the Pearson correlation coefficients of the shape characteristics and crushing force of NF, PF, KF, CF, and OF were calculated, and through a two-tailed T test with a significance level of 0.05, the reliability of the correlation coefficient r is examined, and the results are shown in Figure 7.

It can be seen from Figure 7 that the length, width, thickness, and granularity of NF, KF, PF, CF, and OF are positively correlated with the crushing force, while the equiaxed rate, flake rate, roundness, and sphericity have no significant correlation with crushing force. Among all the shape characteristics that affect the crushing force of fertilizers, the granularity of the fertilizer has the most significant effect on the crushing force.

3.3. Support Vector Machine Regression. Because of the random volatility of the fertilizer characteristic detection process, a support vector machine regression model with certain advantages in fitting small samples and nonlinear problems is used to construct a prediction model of fertilizer characteristics and crushing force.[33,34] In the process of fertilizer shape feature detection, the input variable x_i and output (fertilizer crushing force) s_i of each set of experiments are used to construct a sample space $\{(x_i, s_i), i = 1, 2, 3, ..., n\}$. s_i can be expressed as a nonlinear function model, as shown in eq 13

$$f_s(x) = \omega^T \varphi(x) + b \tag{13}$$

where $\varphi(x)$ is the nonlinear mapping of the input space x, ω^T is the coefficient of the independent variable function, and b is the offset.

To minimize the empirical risk of training errors, ω^T and b are evaluated by the model shown in eq 14

$$R(f) = \min\left(\frac{1}{2}\|\omega\|^2 + \frac{C}{n}\sum_{j=1}^{n} L(y_i, f(x_i))\right) \tag{14}$$

where $R(f)$ is the generalized optimal classification surface function considering the least misclassified samples, C is the penalty factor, and L is the loss function.

Subsequently, the insensitive loss function ε is introduced to evaluate the structural risk minimization. ξ_i and ξ_i^* are defined as slack variables, and the optimization objective can be changed into the following form

$$\begin{cases} \min \dfrac{1}{2}\|\omega\|^2 + C\sum_{i=1}^{n}(\xi_i + \xi_i^*) \\ \text{s. t. } y^i - \omega^T\varphi(x) - b \le \xi^i + \varepsilon \\ \omega^T\varphi(x) + b - y^i \le \xi^{i*} + \varepsilon \\ \xi_i,\ \xi_i^* \ge 0 \end{cases} \tag{15}$$

We introduce the Lagrange equation

https://dx.doi.org/10.1021/acsomega.0c05120
ACS Omega 2021, 6, 3612−3624

Table 3. Evaluation Indexes of Different Fertilizers

Kernel function	NF			PF			KF			CF			OF		
	MAPE	RMSE	R^2	MAPE	RMSE	R^2	MAPE	RMSE	R^2	MAPE	RMSE	R^2	MAPE	RMSE	R^2
RBF	0.065	1.863	0.916	0.080	8.544	0.758	0.170	24.827	0.652	0.090	7.387	0.761	0.073	3.155	0.757
PK	0.135	3.533	0.700	0.095	11.005	0.571	0.222	30.102	0.496	0.101	8.706	0.668	0.079	3.618	0.682
SK	0.191	4.647	0.532	0.100	11.772	0.510	0.527	36.571	0.403	0.181	9.748	0.407	0.116	5.757	0.432
LK	0.069	1.896	0.914	0.096	9.846	0.678	0.179	25.950	0.619	0.094	8.704	0.670	0.078	3.510	0.670

Table 4. Parameter Selection Range of the Support Vector Machine

parameters	NF	PF	KF	CF	OF
C	46.156−92.312	185.198−370.396	217.098−434.196	140.332−280.664	61.862−123.724
σ	0.562−0.841	0.562−0.841	0.562−0.841	0.562−0.841	0.562−0.841
ε	0.0562−0.0841	0.0562−0.0841	0.0562−0.0841	0.0562−0.0841	0.0562−0.0841

$$L := \frac{1}{2}\|\omega\| + C\sum_{i=1}^{n}(\xi_i + \xi_i^*) - \sum_{i=1}^{n}\alpha_i(\varepsilon + \xi_i^* - y_i + \omega^{\mathrm{T}}\varphi(x_i) + b) - \sum_{i=1}^{n}\alpha_i^*(\varepsilon + \xi_i^* - y_i + \omega^{\mathrm{T}}\varphi(x_i) + b) - \sum_{i=1}^{n}(\eta_i\xi_i + \eta_i^* + \xi_i^*) \quad (16)$$

where α_i, α_i^*, ξ_i, $\xi_i^* \geq 0$ are Lagrange multipliers.

We use the Lagrange equation to find the partial derivative of $(\omega, b, \xi_i, \xi_i^*)$, substitute it into eq 16, transform it into a dual optimization problem, and solve to obtain the regression function of the support vector regression machine, as shown in eq 17

$$f_s(x) = \sum_{i=1}^{n}(\alpha_i - \alpha_i^*)K\langle x_i, x_j\rangle + b(j = 1, 2, 3, \ldots, n) \quad (17)$$

where $K\langle x_i, x_j\rangle = \varphi(x_i)\varphi(x_j)$ is the kernel function.

3.4. Optimal Kernel Function Selection. To determine the optimal kernel function of the fertilizer crushing force prediction model, this paper uses LK (Linear Kernel), PK (Polynomial Kernel), RBF (Radial Basis Function), and SK (Sigmoid Kernel) as the kernel functions to construct the prediction model of fertilizer shape characteristics and crushing force and set the MAPE (Mean Absolute Percentage Error), RMSE (root-mean-square error), and R^2 to quantitatively evaluate the prediction performance of the model. The results of each evaluation index for different fertilizers are shown in Table 3. Among them, the evaluation indicators are

$$\mathrm{MAPE} = \frac{1}{n}\frac{\sum_{i,s=1}^{n}|y_i - y_s|}{y_i} \quad (18)$$

$$\mathrm{RMSE} = \sqrt{\frac{1}{n}\sum_{i,s=1}^{n}(y_i - y_s)^2} \quad (19)$$

$$R^2 = 1 - \frac{\sum_{i,s=1}^{n}(y_i - y_s)^2}{\sum_{i,s=1}^{n}(y_i - \overline{y}_s)^2} \quad (20)$$

where y_i is the actual value of crushing force, y_s is the predicted value of crushing force, and $\overline{y}_s$ is the average value of the predicted value of the crushing force.

RMSE is a good measure of prediction accuracy, MAPE can effectively evaluate the volatility between data, R^2 represents the ratio of the explained change to the total change, which is one of the indicators that measure the effectiveness of the established model. Among them, the smaller the value of RMSE and MAPE, the larger the value of R^2, which indicates that the prediction performance of the model is better. According to the data comparison in Table 3, when the kernel function is RBF, the crushing force prediction models of NF, PF KF, CF, and OF have the smallest MAPE and RMSE and the largest R^2, indicating that the model has the highest prediction accuracy, the smallest prediction fluctuation, and the best prediction performance. Therefore, this paper chooses RBF as the kernel function.

3.5. Parameter Optimization of the Prediction Model. In the SVM model with the kernel function of RBF, the penalty parameter C balances the complexity of the model and the degree of approximation error. Its value affects the learning ability of the model. The kernel width σ relates to the radial range of the function, and the parameter ε of the loss function controls the width of the insensitive area of the regression function to the data sample and affects the learning accuracy and generalization ability of the algorithm. It can be seen that the internal parameters of the model affect the predictive performance of the model. To obtain more satisfactory internal parameters of the support vector machine, the parameters C, ε, and σ are optimized by the differential evolution algorithm. The whole optimization process includes three parts: the range determination of optimization parameters, the selection of fitness function, and the algorithm flow.

In the process of optimizing, a larger parameter range will generate more search space and often get better parameter combinations, but it will take more search time. To reduce the search time, this paper calculates the search range of the three optimization parameters to determine the effective search space. We calculate the value ranges of the parameters C, ε, and σ by formulas 21, 22, and 23, respectively. The calculation results are shown in Table 4.

$$C = [|\overline{y} - 3\sigma_t|, |\overline{y} + 3\sigma_t|] \quad (21)$$

$$\sigma = [0.1^{1/z}, 0.5^{1/z}] \quad (22)$$

https://dx.doi.org/10.1021/acsomega.0c05120
ACS Omega 2021, 6, 3612−3624

Table 5. Optimal Parameters of the Support Vector Machine

model parameter		NF	PF	KF	CF	OF
C	before optimization	10.500	10.500	10.500	10.500	10.500
	after optimization	48.166	307.250	234.033	158.634	121.000
σ	before optimization	0.500	0.500	0.500	0.500	0.500
	after optimization	0.576	0.669	0.593	0.826	0.732
ε	before optimization	0.050	0.050	0.050	0.050	0.050
	after optimization	0.0588	0.0674	0.569	0.0840	0.0749

$$\varepsilon = \frac{\sigma}{\sqrt{n}} \tag{23}$$

where $\overline{y}$ is the average value of crushing force, σ_t is the standard deviation of crushing force, and z is the number of parameters that affect fertilizer crushing force.

Considering the possibility that SVM can reduce the generalization error of the model, this paper selects MSE as the fitness function. The minimized MSE of the model output is the goal of optimizing C, ε, and σ, as shown in eq 24

$$\mathrm{MSE} = \frac{1}{n}\sum_{i=1}^{n}(y_i - \overline{y_s})^2 \tag{24}$$

The DE-SVM model is used to train 100 sets of data and iteratively obtain the combination of C, ε, and σ that meet the requirements of the fitness function (minimum MSE). When the predefined maximum number of iterations M is exceeded, the optimization ends. The process of searching for the best internal parameters is as follows:

First we define a population of size N_P, $\{X_i | X_{i,j}^L \le X_{i,j},\ i = 1, 2, ..., N_P;\ j = 1, 2, ..., D\}$, where X_i is the i-th individual and j represents the j-th dimension; $D = 3$, $X_{i,1}$, $X_{i,2}$, $X_{i,3}$ correspond to C_i, ε_i and σ_i, respectively, and the individuals in the population are randomly initialized according to formula 25

$$x_{i,j} = x_{i,j}^L + \mathrm{rand}(0,\ 1)(x_{i,j}^U,\ x_{i,j}^L) \tag{25}$$

where $X_{i,jj}^U$, and $X_{i,jj}^L$ are the upper and lower bounds of the j-th dimension, respectively.

Then, two individuals are randomly selected (the individuals are different from each other); the selected individual vector difference is scaled, and the vector is synthesized with the individual $X_i(g)$ to be mutated to complete the mutation process, as shown in eq 26

$$V_i(g+1) - X_I(g) + F(X_{r1}(g) - X_{r1}(g)) \tag{26}$$

where r_1 and r_2 are random numbers that are not equal to each other and not equal to i in the interval $[1, N_P]$, F is the scaling factor, and g represents the g-th generation in the population change process.

Then, between the individual offspring obtained by the mutation and the corresponding parent, the individual is randomly selected according to formula 27 to realize the crossover of the individual.

$$U_{i,j}(g+1) = \begin{cases} V_{i,j}(g+1) & \text{if } \mathrm{rand}(0,\ 1) \le \mathrm{CR} \\ x_{i,j}(g) & \text{otherwise} \end{cases} \tag{27}$$

where CR is the crossover probability.

Finally, based on the greedy algorithm, we compare the MSE value of the individual and select the individual with a smaller MSE as the new individual, as shown in eq 28

$$X_i(g+1) = \begin{cases} U_i(g+1) & \text{if } f(U_i(g+1)) \le f(X_i(g))) \\ X_i(g) & \text{otherwise} \end{cases} \tag{28}$$

We traverse N_P individuals in the population and perform the abovementioned mutation, crossover, and selection operations in a loop to complete the first iteration. Then, we continue to iterate to M times to obtain the corresponding C, ε, and σ values when the minimum MSE value is generated. The model parameters before and after optimization are shown in Table 5. We substituting the optimized C, ε, and σ values into the fertilizer crushing force prediction model and compare with the prediction model before optimization; the result is shown in Figure 8.

It can be seen from Figure 8 that the models before and after the optimization of different fertilizers can better capture the trends that are in line with actual measurements. Among them, the predicted curve obtained by the optimized model is closer to the actual curve, indicating that the fitting effect of the optimized fertilizer crushing force prediction model is better than that before the optimization.

The normal distribution test was performed on the predicted crushing force of different fertilizers, and it was found that the distribution of the crushing force of the fertilizer belongs to the normal distribution, and the result is shown in Figure 9. Among all fertilizer shape characteristics, fertilizer granularity has the greatest positive correlation with crushing force, and fertilizer granularity can be determined through a standard sieve. Therefore, in the selected fertilizer samples, we first find NF, PF, KF, CF, and OF particles that meet the crushing force distribution range according to formula 29 and then find their granularity distribution range as the inspection range for optimized fertilizer processing. The granularity distribution range of each fertilizer is 4.03−4.74, 3.90−4.73, 4.83−5.83, 4.28−5.34, and 4.33−5.04 mm, respectively.

$$y \ge \overline{y} + \sigma_t \tag{29}$$

3.6. Experimental Verification. In June 2020, the verification test was carried out at the Key Laboratory of Gardening Machinery and Equipment of Shandong Province. We first pass the standard sieve to select the particles that meet the granularity distribution range from the N fertilizer produced by Sinofert Holding Limited, P fertilizer produced by Yuntianhua Group Co., Ltd., K fertilizer produced by Luxi Chemical Group Co., Ltd., compound fertilizer produced by Stanley Agricultural Group Co., Ltd., and organic fertilizer produced by Xinyangfeng Agricultural Technology Co., Ltd., and then randomly sample 20 particles from each fertilizer as verification samples; the actual crushing force of the fertilizer is obtained through experiments, and the P-DE-SVM model is used to predict the crushing force of the fertilizer. The error rate is calculated according to formula 30, and the

https://dx.doi.org/10.1021/acsomega.0c05120
ACS Omega 2021, 6, 3612−3624

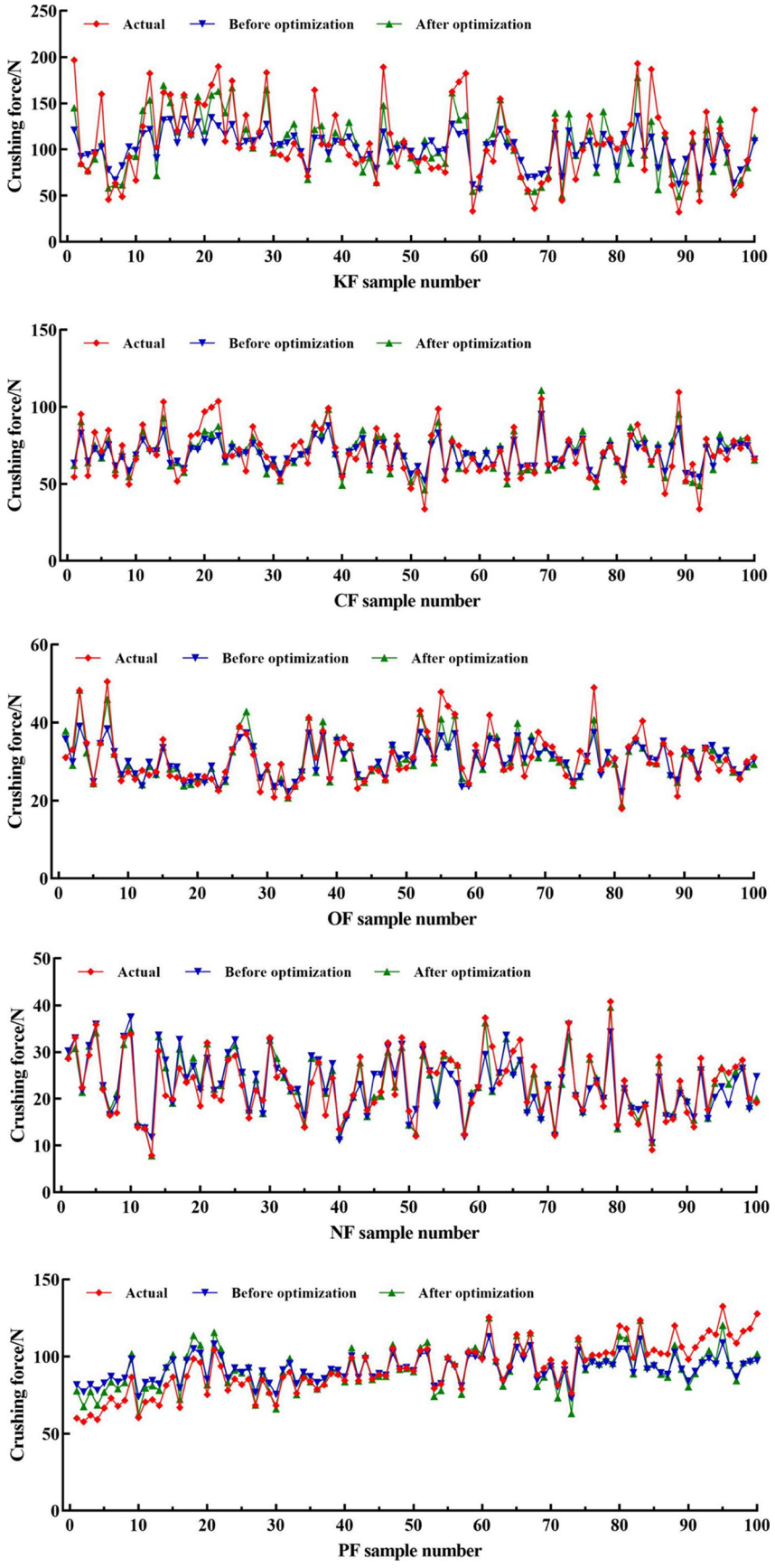

Figure 8. Comparison of prediction models before and after optimization of different fertilizers.

https://dx.doi.org/10.1021/acsomega.0c05120
ACS Omega 2021, 6, 3612−3624

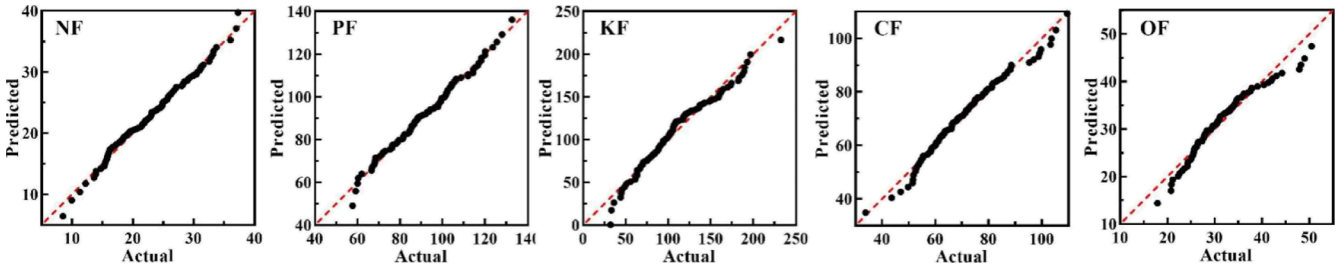

Figure 9. Normal distribution of crushing force of different fertilizers.

Table 6. Verification Test Results

	item	length a/mm	width b/mm	thickness c/mm	granularity d/mm	actual crushing force s_1/N	predicted crushing force s_2/N	error rate e/%
NF	maximum	5.590	5.020	4.270	4.740	37.300	35.570	8.085
	minimum	4.100	3.960	3.500	4.027	25.050	26.582	−8.198
	average	4.673	4.240	3.858	4.240	31.083	30.588	1.188
	range	1.490	1.060	0.770	0.713	12.250	8.988	16.283
	standard deviation	0.372	0.269	0.178	0.193	3.303	2.322	5.284
PF	maximum	5.660	4.590	3.990	4.438	120.000	109.178	9.352
	minimum	4.110	3.760	2.970	3.903	86.650	90.049	−7.173
	average	4.870	4.163	3.445	4.109	102.058	99.815	1.722
	range	1.550	0.830	1.020	0.535	33.350	19.129	16.525
	standard deviation	0.376	0.265	0.310	0.160	10.310	5.862	5.752
KF	maximum	9.490	5.710	4.370	5.669	189.150	169.472	10.900
	minimum	5.710	4.400	2.570	4.826	84.650	91.960	−10.401
	average	7.404	5.089	3.621	5.122	133.758	128.609	2.489
	range	3.780	1.310	1.800	0.844	104.500	77.512	21.301
	standard deviation	0.930	0.437	0.416	0.232	31.793	24.093	7.346
CF	maximum	5.450	5.110	4.580	4.936	103.700	99.823	9.846
	minimum	4.370	4.260	3.480	4.313	61.400	67.124	−9.322
	average	4.709	4.495	4.291	4.491	84.460	81.693	2.920
	range	1.080	0.850	1.100	0.624	42.300	32.699	19.168
	standard deviation	0.305	0.207	0.254	0.159	10.627	8.796	5.274
OF	maximum	5.160	4.980	4.870	4.979	50.500	48.408	8.628
	minimum	4.410	4.330	4.140	4.326	29.450	28.672	−8.879
	average	4.738	4.597	4.466	4.598	36.535	35.748	1.752
	range	0.750	0.650	0.730	0.653	21.050	19.736	17.507
	standard deviation	0.244	0.216	0.209	0.205	5.833	4.889	4.678

accuracy of the fertilizer crushing force model is evaluated using the error rate. The test results are shown in Table 6. The crushing force and error rate distributions of different fertilizers are shown in Figure 10.

$$e = \frac{(s_2 - s_1)}{s_1} \times 100\% \tag{30}$$

where s_1 is the actual measured crushing force, s_2 is the predicted crushing force, and e is the error rate.

The results showed that the maximum error rate of the predicted crushing force of NF, PF, KF, CF, and OF is between −10.401 and 10.900%, indicating the predicted value of the model and the test result are consistent, which verifies the accuracy of the built P-DE-SVM model. After screening through the standard sieve, the average crushing force of NF, PF, KF, CF, and OF were 31.083, 102.058, 133.758, 84.463, and 36.535 N, which were all higher than those of the fertilizers in the test sample without screening. The mean value of force verifies the rationality of the set granularity inspection range.

4. CONCLUSIONS

(1) The shape characteristics of different fertilizers were nondestructively measured by the machine vision method, and the shape characteristics related to the fertilizer crushing force were proposed based on the Pearson correlation coefficient. The experiment results showed that the shape characteristics that affect the crushing force were length, width, thickness, and granularity.

(2) The crushing force prediction model of different fertilizers was constructed based on a support vector machine in which the optimal kernel function was a radial basis function. The experiment results showed that the maximum error rate of the prediction model was between −10.401 and 10.900%, indicating that the

https://dx.doi.org/10.1021/acsomega.0c05120
ACS Omega 2021, 6, 3612−3624

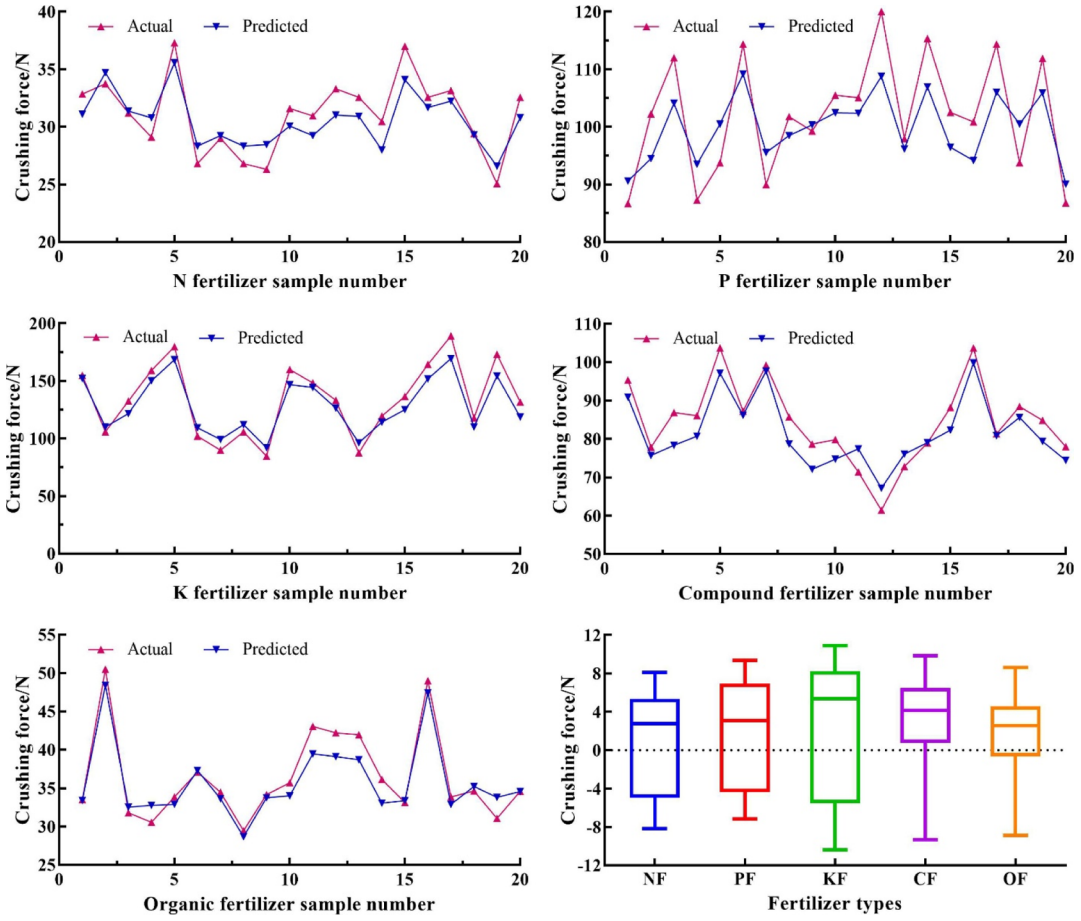

Figure 10. Crushing force and error rate distribution of different fertilizers.

fertilizer crushing force prediction model was accurate and reliable, which provided a theoretical basis for fertilizer production and quality inspection.

(3) The differential evolution algorithm was proposed to optimize the internal parameters of the fertilizer crushing force prediction model, and at the same time, a fertilizer granularity inspection range was calculated. The experimental results exhibited that the average strength of screened samples within the granularity inspection range was higher than the average strength of unscreened samples, indicating the granularity inspection range was reasonable. It would help reduce fertilizer crushing and improve fertilizer utilization to realize the sustainable and clean production of crops.

AUTHOR INFORMATION

Corresponding Author

Jinxing Wang − *College of Mechanical and Electronic Engineering, Shandong Agricultural University, Taian 271018, China; Shandong Provincial Key Laboratory of Horticultural Machinery and Equipment, Taian, Shangdong 271018, China;* orcid.org/0000-0003-3684-3344; Email: jinxingw@168.com

Authors

Hongjian Zhang − *College of Mechanical and Electronic Engineering, Shandong Agricultural University, Taian 271018, China; Shandong Provincial Key Laboratory of Horticultural Machinery and Equipment, Taian, Shangdong 271018, China*

Xuemei Liu − *College of Mechanical and Electronic Engineering, Shandong Agricultural University, Taian 271018, China; Shandong Provincial Key Laboratory of Horticultural Machinery and Equipment, Taian, Shangdong 271018, China*

Shuangxi Liu − *College of Mechanical and Electronic Engineering, Shandong Agricultural University, Taian 271018, China; Shandong Provincial Key Laboratory of Horticultural Machinery and Equipment, Taian, Shangdong 271018, China*

Hao Jiang − *College of Mechanical and Electronic Engineering, Shandong Agricultural University, Taian 271018, China; Shandong Provincial Key Laboratory of Horticultural Machinery and Equipment, Taian, Shangdong 271018, China*

Chunbao Xu − *College of Mechanical and Electronic Engineering, Shandong Agricultural University, Taian 271018, China; Shandong Provincial Key Laboratory of Horticultural Machinery and Equipment, Taian, Shangdong 271018, China*

Complete contact information is available at: https://pubs.acs.org/10.1021/acsomega.0c05120

Notes

The authors declare no competing financial interest.

https://dx.doi.org/10.1021/acsomega.0c05120
ACS Omega 2021, 6, 3612−3624

■ ACKNOWLEDGMENTS

This work was supported by the National Key Research and Development Plan of China (2016YFD0201104), the National Apple Industry Technology System Project of China (CARS-27), and the Rice Industry Innovation Team of Modern Agricultural Technology System in Shandong Province.

■ REFERENCES

(1) Putra, R. C.; Hidayah, S. N.; Purwanto, B. H. Influence of goat manure and Azolla on soil properties, nitrogen use efficiency, growth and yield of organic rice farming in Indonesia. *IOP Conf. Ser. Earth Environ. Sci.* **2018**, *215*, 99−123.

(2) Chen, J.; Lü, S.; Zhang, Z.; Zhao, X.; Li, X.; Ning, P.; Liu, M. Environmentally friendly fertilizers: A review of materials used and their effects on the environment. *Sci. Total Environ.* **2018**, *613*−*614*, 829−839.

(3) Kabiri, S.; Tran, D. N. H.; Baird, R.; McLaughlin, M. J.; Losic, D. Revealing the dependence of graphene concentration and physicochemical properties on the crushing strength of co-granulated fertilizers by wet granulation process. *Powder Technol.* **2020**, *360*, 588−597.

(4) Kasmadi, K.; Nugroho, B.; Sutandi, A.; Anwar, S. Filter cake utilization as filler of 15-15-15+5S compound fertilizer: particle size distribution and granule crushing strength properties. *Reaktor* **2019**, *19*, 145−151.

(5) Payan, M.; Khoshghalb, A.; Senetakis, K.; Khalili, N. Effect of particle shape and validity of G(max) models for sand: A critical review and a new expression. *Comput. Geotech.* **2016**, *72*, 28−41.

(6) Vangla, P.; Roy, N.; Gali, M. L. Image based shape characterization of granular materials and its effect on kinematics of particle motion. *Granul. Matter* **2018**, *20*, 6.

(7) Altuhafi, F.; O'sullivan, C.; Cavarretta, I. Analysis of an image-based method to quantify the size and shape of sand particles. *J. Geotech. Geoenviron. Eng.* **2012**, *139*, 1290−1307.

(8) Antony, S. J.; Kuhn, M. R. Influence of particle shape on granular contact signatures and shear strength: new insights from simulations. *Int. J. Solid Struct.* **2004**, *41*, 5863−5870.

(9) Hou, H. M.; Cui, Q. L.; Guo, Y. M. Effects of moisture contents of threshed materials from whole-feeding combine for foxtail millet on their suspension characteristics. *Trans. Chin. Soc. Agric. Eng.* **2018**, *34*, 29−35.

(10) Xu, L. Z.; LI, Y.; LI, Y. M.; Chai, X. M.; Qiu, J. Research progress on cleaning technology and device of grain combine harvester. *Trans. Chin. Soc. Agric. Mach.* **2019**, *50*, 1−16.

(11) Kan, H. F.; Su, J. L.; Tang, C. J. Anti-caking measure for compound fertilizer by acid ammoniation process and its application. *Phosphate Compd. Fert.* **2016**, *31*, 31−32.

(12) Hofstee, J. W.; Huisman, W. Handling and spreading of fertilizers part1: Physical properties of fertilizer in relation to particle motion. *J. Agric. Eng. Res.* **1990**, *47*, 213−234.

(13) Cao, S.; Wang, S.; Wang, Y.; Feng, G.; Yan, L.; Yuan, Y.; Du, S.; Gao, Q. Physical properties and suitability of common base fertilizers for blending fertilizers. *J. Plant. Nutr. Fert.* **2019**, *25*, 647−653.

(14) Basu, S. K.; Kumar, N. Mathematical model and computer-simulation for release of nutrients from coatedfertilizer granules. *Math. Comput. Simulat.* **2008**, *79*, 634−646.

(15) Terry, D. L. Distribution of fertilizer sales in Kentucky. *Coll. Agric.* **1990**, *12*, 12−15.

(16) Hoffmeister, G.; Watkins, S. C.; Silverberg, J. Fertilizer Consistency, Bulk Blending of Fertilizer Material: Effect of Size, Shape, and Density on Segregation. *J. Agric. Food Chem.* **1964**, *12*, 64−69.

(17) Fernlund, J. M. R. Image analysis method for determining 3-D shape of coarse aggregate. *Cem. Concr. Res.* **2005**, *35*, 1629−1637.

(18) Zhang, J. F.; Ye, J. B.; Chen, J. S.; Li, S. L. A preliminary study of measurement and evaluation of break stone grain shape. *Rock Soil Mech.* **2016**, *37*, 343−349.

(19) Abrougui, K.; Gabsi, K.; Mercatoris, B.; Khemis, C.; Amami, R.; Chehaibi, S. Prediction of organic potato yield using tillage systems and soil properties by artificial neural network (ANN) and multiple linear regressions (MLR). *Soil Tillage Res.* **2019**, *190*, 202−208.

(20) Barman, U.; Choudhury, R. D. Soil texture classification using multi class support vector machine. *Inform. Process Agric.* **2020**, *7*, 318−332.

(21) Iznaga, A. C.; Orozco, M. R.; Alcantara, E. A.; Pairol, M. C.; Díaz-Sicilia, Y. E.; Baerdemaeker, J.; Saeys, W. Vis/NIR spectroscopic measurement of selected soil fertility parameters of Cuban agricultural Cambisols. *Biosyst. Eng.* **2014**, *125*, 105−121.

(22) Stevens, A.; Nocita, M.; Tóth, G.; Montanarella, L.; van Wesemael, B. Prediction of soil organic carbon at the European scale by visible and near infraRed reflectance spectroscopy. *PLoS One* **2013**, *8*, No. e66409.

(23) Lu, J.; Zhang, Z. K.; Wu, Z. Q.; Ma, J. Y.; Liao, X. P.; Hu, S. S. Prediction of surface roughness for compacted graphite cast iron based on support vector machine. *Surf. Technol.* **2020**, *49*, 339−346.

(24) Li, Z.-m.; Gui, W.-h.; Zhu, J.-y. Fault detection in flotation processes based on deep learning and support vector machine. *J. Cent. S. Univ.* **2019**, *26*, 2504−2515.

(25) LI, B. X.; Wang, W.; Chen, M. Y.; Ye, M. Isometric ratio, roundness and Sphericity of coarse aggregates and their relationship. *J. Build. Mater.* **2015**, *18*, 531−536.

(26) Scheibelhofer, O.; Besenhard, M. O.; Piller, M.; Khinast, J. G. Comparing particle size distributions of an arbitrary shape. *Powder Technol.* **2016**, *294*, 134−145.

(27) Mora, C. F.; Kwan, A. K. H. Sphericity, shape factor, and convexity measurement of coarse aggregate for concrete using digital image processing. *Cem. Concr. Res.* **2000**, *30*, 351−358.

(28) Rakotonirina, A. D.; Delenne, J.-Y.; Radjai, F.; Wachs, A. Grains3D, a flexible DEM approach for particles of arbitrary convex shape—Part III: extension to non-convex particles modelled as glued convex particles. *Comput. Part. Mech.* **2019**, *6*, 55−84.

(29) Masad, E.; Olcott, D.; White, T.; Tashman, L. Correlation of fine aggregate imaging shape indices with asphalt mixture performance. *J. Transp. Res. Board* **2001**, *1757*, 148−156.

(30) Fu, J. J.; Wang, C. Y.; Huang, Z. W.; Chen, D. M. Classification research and types of slow controlled release fertilizers (SRFs) used - a review. *Commun. Soil Sci. Plant Anal.* **2018**, *49*, 2219−2230.

(31) Pforte, F.; Selbeck, J.; Hensel, O. Comparison of two different measurement techniques for automated determination of plum tree canopy cover. *Biosyst. Eng.* **2012**, *113*, 325−333.

(32) Mollenhorst, H.; de Haan, M. H. A.; Oenema, J.; Kamphuis, C. Field and crop specific manure application on a dairy farm based on historical data and machine learning. *Comput. Electron. Agric.* **2020**, *175*, 105599.

(33) Morellos, A.; Pantazi, X.-E.; Moshou, D.; Alexandridis, T.; Whetton, R.; Tziotzios, G.; Wiebensohn, J.; Bill, R.; Mouazen, A. M. Machine learning based prediction of soil total nitrogen, organic carbon and moisture content by using VIS-NIR spectroscopy. *Biosyst. Eng.* **2016**, *152*, 104−116.

(34) Esfandiarpour-Boroujeni, I.; Karimi, E.; Shirani, H.; Esmaeilizadeh, M.; Mosleh, Z. Yield prediction of apricot using a hybrid particle swarm optimization-imperialist competitive algorithm-support vector regression (PSO-ICA-SVR) method. *Sci. Hortic.* **2019**, *257*, 108756.

https://dx.doi.org/10.1021/acsomega.0c05120
ACS Omega 2021, 6, 3612−3624